Journal of Materials Chemistry A

PAPER

View Article Online
View Journal | View Issue

Cite this: J. Mater. Chem. A, 2016, 4, 938

Hybrid-dimensional magnetic microstructure based 3D substrates for remote controllable and ultrafast water remediation†

Ran Du,[a] Qingliang Feng,[ab] Huaying Ren,[ac] Qiuchen Zhao,[a] Xin Gao[a] and Jin Zhang*[a]

Received 29th October 2015
Accepted 26th November 2015

DOI: 10.1039/c5ta08723f

www.rsc.org/MaterialsA

In the field of water remediation, a 3D hydrophobic material with both remote controllability and high oil adsorption performance is highly desirable. To achieve it, magnetic components and microstructures are most likely involved. However, the simple enrolling of magnetic materials always results in quite low adsorption capacity. Additionally, the control of microstructures on 3D materials is immature, which limits the improvement of water/oil selectivity and oil adsorption speed. Herein, we devised 0D/2D hybrid dimensional magnetic microstructures with a well-defined morphology on melamine foams, which provided magnetism for remote controllability and highly rough surfaces for substantially enhanced water/oil selectivity. Hence, the resultant materials acquired magnetic-driven properties and superhydrophobicity/superoleophilicity simultaneously. Thus, they possess controllable, ultrafast, and high throughput oil uptake ability and high oil/water separation performance. The present strategy may open a new avenue to devise high-performance magnetic 3D assemblies for water remediation.

Introduction

Due to the increasingly aggravated water pollution around the world, the study on water remediation, such as oil/water separation and selective oil uptake is becoming more and more important.[1,2] In the last few years, three-dimensional (3D) hydrophobic/oleophilic materials (3D-HOMs) have appeared as rising stars in water remediation, for their promising use in both oil uptake and water/oil separation with high processing capacity.[3–5] A series of 3D substrates based on carbon nanomaterials,[6–12] microporous sponges,[13,14] commercial foams or sponges, and metal foams[1,2,15–18] have been fabricated, which showed high oil adsorption capacity up to 1000 times and excellent oil/water separation performance. Very recently, the elaborate design of microstructures on 3D substrates has also been considered in a few cases,[3,5,19] further promoting the performance of water remediation by improving the water/oil selectivity.

On the other hand, to facilitate the handling of 3D-HOMs during the water purification process and collection after use, it is desirable to impart remote controllability to materials. For this purpose, one feasible way is to integrate magnetic components in 3D-HOMs. In recent years, several studies have demonstrated magnetism integration in 3D networks to produce magnetic-driven sorbents.[20–28] For example, Gui *et al.*[22] fabricated magnetic carbon nanotube (CNT) based sponges by *in situ* filling magnetic Fe nanowires into the inner cavity of CNTs during the chemical vapor deposition process, where the magnetic components were permanently integrated, thus ensuring excellent recyclability of the resultant materials. However, the magnetism integration and oil adsorption performance of these materials often showed a tradeoff effect. For most of the studies, the magnetic components are simply enrolled for magnetism integration, which is at the expense of density increase of original materials thus reducing the adsorption capacity.[7] Actually, on average, the maximum oil adsorption capacity of the magnetic 3D-HOMs is only about 30 times the weight gain, far less than that of conventional 3D-HOMs (typically over 100 times the weight gain). A few studies have been devoted to solve this problem by fabricating low-density materials.[21,27] For example, Chen *et al.*[21] prepared ultralight foams (density < 5 mg cm^{-3}) by pyrolyzing metal grafted polyurethane foams, thus achieving an oil adsorption capacity of over 100 times the weight gain. In another work, Kong *et al.*[27] fabricated iron oxide networks by devising unique hierarchical macroporous/mesoporous structures, which greatly reduced the density of resultant materials thus obtaining a high adsorption capacity of over 150 times the weight gain.

[a]Center for Nanochemistry, Beijing National Laboratory for Molecular Sciences, Key Laboratory for the Physics and Chemistry of Nanodevices, State Key Laboratory for Structural Chemistry of Unstable and Stable Species, College of Chemistry and Molecular Engineering, Peking University, Beijing 100871, P.R. China. E-mail: jinzhang@pku.edu.cn

[b]School of Chemistry and Chemical Engineering, Lanzhou University, Lanzhou 730000, P. R. China

[c]Academy for Advanced Interdisciplinary Studies, Peking University, Beijing 100871, China

† Electronic supplementary information (ESI) available: Experimental details including thermogravimetric analysis, contact angle measurements, SEM images, *etc.* See DOI: 10.1039/c5ta08723f

However, more facile synthetic routes, higher oil/water selectivity, and better water remediation performance are still needed to be met for practical use. Therefore, it is highly desirable and challenging to fabricate 3D-HOMs that simultaneously possess remote controllability and high processing capacity in water remediation.

The elaborate engineering of the microstructures on 3D substrates can serve as a feasible way to solve the above problems. From the fundamental mechanism, the oil/water selectivity could be significantly improved by introducing suitable microstructures, which are capable of enhancing the surface roughness thus amplifying the intrinsic wettability of materials towards both water and oil.[29] In this way, the original 3D-HOMs could be transformed into superhydrophobic/superoleophilic materials by imparting appropriate microstructures, thus increasing the water/oil selectivity. Additionally, the increase of the surface roughness can also induce increased Laplace pressure, thereby accelerating the oil adsorption and promoting the adsorption capacity. However, the control of non-magnetic microstructures on 3D materials is still immature, let alone the fine engineering of magnetic microstructures on 3D substrates.

On this basis, we assumed that engineering magnetic materials into appropriate microstructures on 3D substrates subtly may provide a new way to solve the above problem by simultaneously providing magnetism for remote control and microstructures for enhancing the oil/water selectivity. Herein, we fabricated unique 0D/2D hybrid dimensional magnetic microstructures with well-defined morphology, *i.e.* cobalt-based 2D micrometre-size sheets composed of zero-dimensional (0D) nanometre-size particles on commercial melamine foams (MF), *via* the combination of controlled precipitation of cobalt(II) ions and reductive annealing. The theoretical calculations showed that these hybrid-dimensional microstructures can dramatically enhance the surface roughness (R_f) up to 6.29, since the apparent R_f is determined by the multiplication of the surface roughness of each dimension, *i.e.* $R_f(R_{f1}, R_{f2}) = R_{f1} \times R_{f2}$. Thus, the water/oil selectivity can be greatly enhanced. After a simple vapor deposition process assisted by polydimethylsiloxane (PDMS), a hybrid-dimensional magnetic microstructure based foam with both remote controllability and superhydrophobicity/superoleophilicity (MM-RSF) was obtained. Together with mechanical flexibility inherited from original melamine foam, the resultant material exhibited not only ultrafast selective oil uptake with high capacity (60–160 times of its weight), good recyclability and magnetic-driven properties, but also excellent oil/water separation performance with an efficiency >99%.

Results and discussion

Synthesis and basic characterization

The synthetic route is illustrated in Fig. 1a, including (1) cobalt(II) hydroxide loading by controlled precipitation of cobalt(II) acetate, (2) reductive annealing, and (3) PDMS vapor deposition. By this method, the micrometre-sized cobalt(II) hydroxide 2D sheets were introduced first on MF surfaces in step (1) to produce $Co(OH)_2$ loaded foam (MF-C), providing the primary microstructures on MF. Then the 2D cobalt(II) hydroxide sheets were transformed to magnetic cobalt nanoparticles in step (2), accounting for magnetism integration and further enhancement of the surface roughness (the resultant magnetic melamine foam is denoted as MMF). Finally, in step (3), the MMF was coated with a low-energy PDMS layer to acquire intrinsic chemical hydrophobicity, thus obtaining superhydrophobic magnetic melamine foam (MM-RSF). As shown in Fig. 1b, the MM-RSF showed two-level structures, *i.e.* several tens of micrometre-sized porous surface (the first-order structure) provided by original foams and the hierarchical micro/nano-sized structure (the second-order structure) provided by nanoparticle composed cobalt sheets. In this design, functional microstructures (the second-order structure) are naturally introduced to impart dual functions to materials, *i.e.* providing high surface roughness for amplification of the intrinsic wettability and integrating magnetism for remote controllability. In combination with low-energy PDMS coating, the resultant MM-RSF simultaneously acquired superhydrophobicity and magnetism.

As shown in Fig. 2a–d and S1,† the morphology evolution during the MM-RSF preparation was revealed by scanning electron microscopy (SEM) and transmission electron microscopy (TEM). The pristine MF exhibited interconnected macroporous structures with the pore sizes of several tens of micrometres. However, the surface of MF is plain on the magnified scale. After the loading process in step (1), MF surfaces were entirely covered by 2D vertically aligned cobalt(II) hydroxide micrometre-sized sheets. Both magnified SEM and TEM images (Fig. 2c & S1c†) of cobalt(II) hydroxide sheets showed very smooth surfaces. The formation of such smooth sheets can be attributed to the controlled precipitation of cobalt(II) acetate enabled by epichlorohydrin, where the latter can serve as a relatively inert proton scavenger thus releasing OH^- in a controllable manner.[30,31] In this way, the $Co(OH)_2$ can slowly develop in a near-equilibrium state, finally forming regular shapes. Additionally, the slow loading process is also crucial to realize complete diffusion inside the foam thereby generating uniform microstructures throughout the whole 3D networks. In contrast, the rapid precipitation process induced by a strong base (potassium hydroxide) not only resulted in uncontrollable rough surfaces (Fig. S2†), but also was unable to achieve uniform loading on 3D substrates.

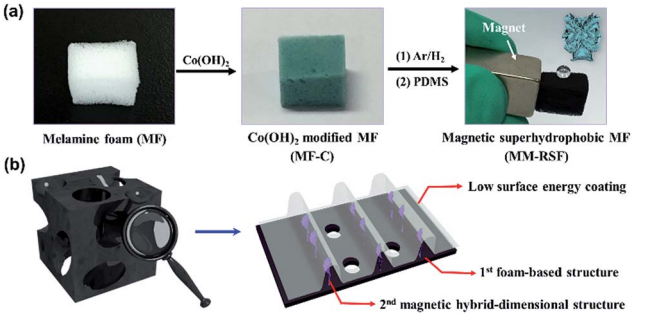

Fig. 1 (a) Illustration of the synthetic strategy and the corresponding digital photos of the material in each step. (b) The demonstration of hierarchical structures of MM-RSF.

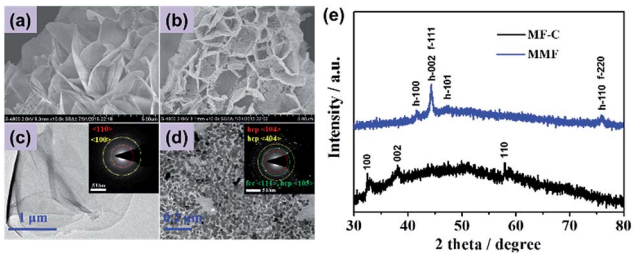

Fig. 2 SEM images and TEM images of (a) and (c) MMF and (b) and (d) MM-RSF, respectively. Insets in (c) and (d) are the corresponding SAED patterns. (e) The powder XRD patterns of loading matter on MF-C and MMF. In (e), h represents hcp cobalt while f represents fcc cobalt.

After reductive annealing, the cobalt(II) hydroxide was converted to ferromagnetic cobalt, which can be verified by selected area electron diffraction (SAED) and powder X-ray diffraction (XRD) (Fig. 2c–e).[32,33] By both thermogravimetric (TG) and inductively coupled plasma atomic emission spectrometry (ICP-AES) analysis, the loading amount of cobalt was determined to be ~20 wt%. Interestingly, accompanied by a chemical reduction process under "dry" conditions, the 2D sheets (several millimetres) were converted to the 0D nanoparticles (several tens of nanometres) without collapse, resulting in the final hierarchical 0D/2D micro/nanostructure with much more enhanced roughness than that of the sole sheet structure. Additionally, the cobalt particles can also impart great magnetism in MF because of their intrinsic high magnetism. Actually, the saturation magnetization of bulk Co (~162 emu g^{-1})[34] is much higher than that of nickel (~58 emu g^{-1})[35] and spinel ferrite Fe_3O_4 (92 emu g^{-1}).[36] As a result, the as-obtained MMF exhibited a quite high saturation magnetization of ~49.2 emu g^{-1}.

Finally, PDMS was coated on the MMF *via* a facile vapor deposition process[7,37] for 15 minutes at 235 °C, during which a conformal layer following the original morphology of MMF was formed (Fig. S1e and f†). It should be noted that although the as-prepared cobalt on MMF is not stable in air at elevated temperatures, the simultaneously deposited PDMS layer can effectively prevent cobalt from deterioration. As evidenced from XRD (Fig. S4†), the cobalt showed considerable oxidation (the appearance of peaks of Co_3O_4 and CoO) after heating alone while minimal oxidation by co-heating with PDMS. In this way, both the magnetism and the hierarchical micro/nanostructures of cobalt are preserved after PDMS modification, enabling resultant MM-RSF to simultaneously possess superhydrophobicity and adequate magnetism. Notably, even after metal loading and PDMS coating, the resultant MM-RSF still possesses a low density of ~13.9 mg cm^{-3}, comparable to that of nitrogen-doped carbon nanotube aerogels (13.4 mg cm^{-3})[8] and spongy graphene (12 ± 5 mg cm^{-3}),[38] and much lighter than porous polymer aerogels (~30–60 mg cm^{-3}),[13,14] which was expected to possess good performance in oil uptake.

Superhydrophobicity of MM-RSF

The hydrophobic properties of resultant materials were first characterized by static water contact angle measurements (Fig. 3a and S5†). The MM-RSF possessed a much higher water contact angle (157.8°) than PDMS-coated pristine MF (135.2°) and many other 3D hydrophobic materials without elaborate microstructure engineering. The remarkable superhydrophobicity can be attributed to the high surface roughness provided by the elaborately devised hierarchical 0D/2D micro/nanostructure. This was further confirmed by the theoretical analysis. As shown in Fig. S6,† for such a hierarchical structure, a multiplication rule was adapted to the surface roughness calculation; thus a considerably high roughness of ~6.29 was obtained. Thereby, the hydrophobicity was remarkably amplified by this highly rough surface. At the same time, superoleophilicity was also acquired in MM-RSF, evidenced from an oil contact angle of 0° (Fig. 3b).

Additionally, the superhydrophobicity of MM-RSF can also be reflected by its low water sliding angle (~9°), fast water rolling process on the surface, and significant water repellency during washing (Fig. 3e, Movie S1†). Moreover, the water droplet can experience two bounces on the surface during the water impact experiment (Fig. S7 and S8†), suggesting remarkable water repellency among soft substrates.[39] Apart from superhydrophobicity, MM-RSF also inherits excellent magnetism from MMF (Fig. S9†), facilitating remote handling. In fact, MM-RSF can even freely rotate when triggered by using a normal magnetic stirrer (Movie S2†). Notably, both the superhydrophobicity and magnetism of the MM-RSF can be well retained after treatment in either a high temperature (200 °C in air) or low temperature (−196 °C in liquid nitrogen) environment (Fig. S10†), enabling its applications under harsh conditions.

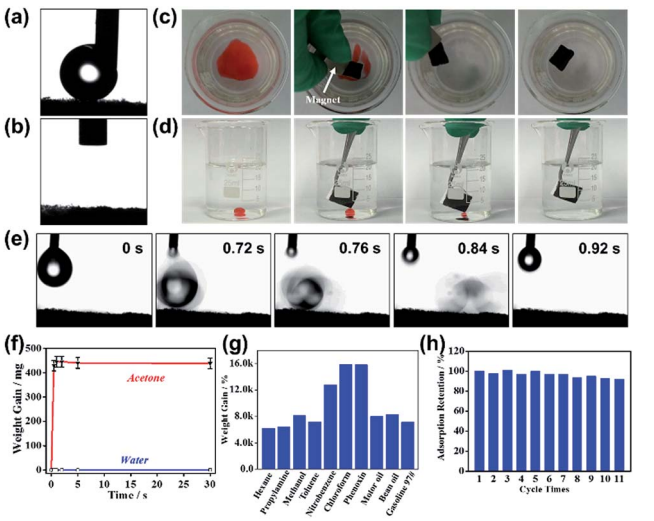

Fig. 3 The static contact angle of (a) water and (b) toluene on MM-RSF. (c) On-water and (d) under-water sorption of organic solvents by MM-RSF, respectively. For on-water sorption, a magnet was used to control the motion of MM-RSF. (e) The snapshots of the water droplet rolling process on MM-RSF (the substrate was tilted by 3°). (f) The time-dependent sorption behaviour of MM-RSF towards acetone (red) and water (blue). (g) The sorption capacity of MM-RSF towards different organic solvents and oils. (h) The sorption capacity retention of MM-RSF after regeneration by directly heating.

Water remediation

Oil adsorption. Bearing both remote controllability and remarkable superhydrophobicity/superoleophilicity, MM-RSF can serve as one of the ideal candidates for water remediation. As shown in Fig. 3b and c, due to ultrahigh water/oil selectivity, MM-RSF can be directly used as an adsorbent for rapid and selective oil removal either on water or under water driven by a magnet. Notably, because of the synergistic effect of fast mass transportation provided by the first-order macroporous structures of MF and much enhanced Laplace pressure provided by hierarchical second-order micro/nanostructures, the oil droplets could quickly wet the surface of MM-RSF and then freely transport in the internal 3D networks. In this way, the MM-RSF can not only exhibit an ultrafast oil uptake behaviour (Movie S3†), but also allow the full use of the pores inside the foam. As shown in Fig. 3f, saturated adsorption can be achieved within 1 s, which is much faster than that of microporous polymer aerogels (over 1 min) and magnetic polyurethane foams (~6 s).[14,20] The adsorption capacity of MM-RSF towards a series of organic solvents and oils was measured, showing a weight gain of 60–160 times (Fig. 3g), which is higher than that of a wide range of polymer sponges or aerogels (13–143 times),[2,13,14,21,23,40] although the value is still lower than that of expensive carbon nanotube sponges (80–180 times) and some carbon nanotubes or graphene based aerogels (up to 1000 times).[6,7,10,12] Additionally, the adsorption capacity of MM-RSF stands out among those of most reported magnetic sponges.[20–24] The high adsorption capacity can be attributed to the enhanced Laplace pressure induced by the elaborately fabricated microstructures, from which the oil was forced to penetrate into the foam rapidly thus enabling the full utilization of the pores inside 3D networks. Moreover, thanks to the excellent mechanical flexibility inherited from MF (Fig. S11†), the MM-RSF can be regenerated by either direct heating in air at 100 °C or squeezing after oil uptake with a good capacity retention (Fig. 3h & S12†), enabling its recycling use.

Oil/water separation. Apart from the selective oil adsorption, the MM-RSF can also serve as the filter for oil/water separation (Fig. 4). Compared with 2D superhydrophobic substrates or 3D hard substrates (*e.g.* hydrophobic copper foams[4,5]), the MM-RSF can not only provide a long flowing path to improve the separation efficiency and capacity, but also facilitate easy handling and performance enhancing. The high separation performance of MM-RSF can be explained from the mechanism during the oil/water separation process. When water was dropped on the filter, it was blocked by the Laplace pressure (F_L) generated from the superhydrophobic surface of MM-RSF (Fig. 4a). If there is only one water droplet on MM-RSF (just like the case for water contact angle measurements), the gravity of droplet (G) can be balanced by the F_L. With increasing water column, the same water droplet will experience increased static pressure (F_p) generated by other water droplets above it (the direction is the same as G), which forced the droplet to wet the substrate thus causing Wenzel-to-Cassie state transition.[41] Since the substrate cannot provide the sufficient F_L to balance $G + F_p$, the water droplet will penetrate the top surface and move to the next surface below it. The filter will finally lose the separation ability

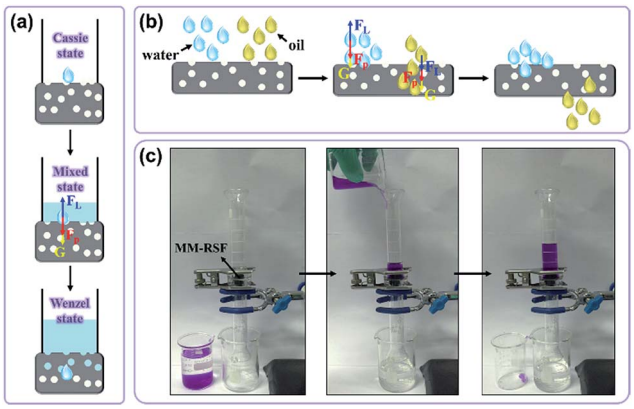

Fig. 4 (a) The analysis of the Cassie-to-Wenzel state transition with increasing height of the water column. (b) The demonstration and force analysis of water and oil droplets during the separation process. In (a) and (b), F_L refers to the Laplace pressure induced by the substrate, F_p refers to the experienced static pressure of the target droplet, and G refers to the gravity of the target droplet. (c) The digital photos of the oil/water separation process by using MM-RSF as the filter.

when all surfaces are wetted by the water. For the 2D filter, the small thickness means fewer available surfaces to resist the water penetration, thus lowering the separation capacity. For the 3D filter, there are many replaceable and interconnected superhydrophobic surfaces beneath the top one. Hence, to completely penetrate the whole substrate, a very high F_p (*i.e.* intrusion pressure F_i) is required. This means that the 3D substrate can support a much higher water column than the thin 2D substrate, enabling its large processing capacity.

On the other hand, considering the state of oil during the separation process (Fig. 4b), the direction of F_L is in opposition to G because of the superoleophilicity of the substrate, thus causing rapid penetration of oil. After the substrate is completely wetted by the oil, the original PDMS coating will be replaced by the oil layer, which can also repel the water because of its immiscibility (this can be evidenced from the high water contact angle of MM-RSF under the oil, see Fig. S13†). In this way, within the intrusion pressure, the oil can be selectively separated from the water. As shown in Fig. 4c, the oil/water mixture (hexane was used to represent oil) can be easily separated by using MM-RSF as the filter, and a separation ratio higher than 99% was obtained using our previously reported method.[5,14] More importantly, due to the mechanical flexibility of MM-RSF, the separation capacity and efficiency can be easily improved by stacking several MM-RSFs together as the filter.

Conclusions

In summary, by elaborately devising and fabricating hybrid-dimensional magnetic microstructures on 3D substrates, a remote controllable and superhydrophobic/superoleophilic melamine foam was facilely prepared. By the combination of controlled precipitation and reductive annealing, a unique 0D/2D hybrid-dimensional cobalt-based microstructure was fabricated on the 3D porous melamine foam, providing both

substantially high surface roughness for enhanced oil/water selectivity and magnetic properties for remote controllability. It should be noted that the elaborately devised hybrid-dimensional microstructures can sharply enhance the apparent surface roughness, because the R_f is determined by the multiplication of surface roughness contributed by each dimension. In the next step, the conformal coating of the hydrophobic PDMS layer generated the MM-RSF that simultaneously enjoyed superhydrophobicity/superoleophilicity and considerable magnetic properties, which showed great potential in both ultrafast, magnetic-driven, and recyclable oil uptake (60–160 times the weight gain) and highly efficient oil/water separation (separation ratio > 99%). The presented method may open a new door for intentionally devising high-surface-roughness magnetic 3D substrates and fabricating high-performance, remote controllable 3D-HOM for water remediation.

Experimental

General

All reagents, such as cobalt acetate tetrahydrate and epichlorohydrin were purchased from commercial suppliers (Alfa-Aesar, TCI or Aladdin Chemistry Co., Ltd.) and used without further purification. The melamine foams were obtained from SINOYQX. Thermogravimetric analysis (TGA) was conducted by using a Q600 STD with a heating rate of 10 K min^{-1} in air or nitrogen. Inductively coupled plasma atomic emission spectrometry (ICP-AES) analysis was conducted using Prodigy7 to determine the cobalt element. Mechanical tests were carried out by using a model 3342 Instron Universal Testing Machine equipped with two flat-surface compression plates and a 100 N load cell. The top plate travelled at a speed of 5 mm min^{-1} for the normal compressible stress–strain test, and 50 mm min^{-1} for loading–unloading cycles. Contact angle measurements were directly conducted on the aerogel at room temperature. The data were collected by using OCA20 (Dataphysics). More than five positions were measured per sample to obtain a mean contact angle. The advancing and receding contact angles were measured by using dispensing and retracting water at a rate of ~1.0 μl s^{-1}. The water impact experiment is conducted by dropping a water droplet (~6 μl) from a ~4 cm height, and then the snapshots were taken by using a high-speed camera (~403 fpm). The impact velocity is calculated to be ~88.5 cm s^{-1}.

Preparation of MM-RSF

The melamine foam (MF) was first dropped into the cobalt acetate tetrahydrate aqueous (0.1 M) containing epichlorohydrin (10 vol%) and heated at 50 °C for ~24 hours. Then the sample was washed with water and frozen at −18 °C in a refrigerator for at least 12 hours before freeze drying for 24 hours, giving rise to cobalt(II) hydroxide loaded melamine foam (MF-C). Then, the dried sample was transferred into a quartz tube and annealed at 350 °C for 1 h under a flow of Ar/H_2 of 300/50 (sccm), thus producing cobalt-loaded magnetic melamine foam (MMF). The resultant MMF was further modified by polydimethylsiloxane (PDMS) vapor deposition. In short, MMF was co-heated with PDMS at 235 °C for 15 minutes in a sealed container, thus creating superhydrophobic and magnetic melamine foam (MM-RSF).

Electron microscopy

Scanning electron microscopy (SEM) was performed on a Hitachi S-4800 field-emission-gun scanning electron microscope (FE-SEM). Transmission electron microscopy (HRTEM) analysis was carried out by using a Tecnai T20 at 200 kV. The microstructures loaded on the MF were transferred to the ethanol solution by sonication for long hours. Then the samples were prepared by dropping the ethanol dispersion onto carbon coated copper grids and drying at ambient temperature.

Oil uptake measurements

Typically, a piece of MM-RSF (*ca.* 2 mg) was dropped into organic solvent or oil for several hours to achieve complete adsorption equilibrium. Then the weight gain (%) was calculated by

$$q_m = 100 \times (m - m_0)/m_0$$

where m_0 and m represent the mass of MM-RSF before and after adsorption, respectively. The regeneration of MM-RSF was achieved by either heating at ~100 °C for several minutes or squeezing using tweezers.

Oil/water separation

A piece of MM-RSF (thickness ~ 4 mm) was used as the filter and assembled into a separation device as in our previous report. In brief, MM-RSF was sandwiched between two hollow glass-made cylinders with a clamp. The oil/water mixture was prepared by mixing the hexane and deionized water (dyed by using xylenol orange) together. For measurement, the oil/water mixture (50 ml, o/w: 4/1) was directly dropped on the separator from the beaker. When the mixed solution went through the separator, the water was selectively blocked while the hexane could easily go through, thus achieving separation.

Acknowledgements

This work was supported by NSFC (20903009, 50972001, 20725307 and 50821061) and MOST (2011CB932601). Supporting Information is available online from Wiley InterScience or from the author.

Notes and references

1 C. Ruan, K. Ai, X. Li and L. Lu, *Angew. Chem., Int. Ed.*, 2014, **53**, 5556.
2 Y. Gao, Y. S. Zhou, W. Xiong, M. Wang, L. Fan, H. Rabiee-Golgir, L. Jiang, W. Hou, X. Huang and L. Jiang, *ACS Appl. Mater. Interfaces*, 2014, **6**, 5924.
3 R. Du, X. Gao, Q. Feng, Q. Zhao, P. Li, S. Deng, L. Shi and J. Zhang, *Adv. Mater.*, 2015, DOI: 10.1002/adma.201504542.
4 D. Zang, C. Wu, R. Zhu, W. Zhang, X. Yu and Y. Zhang, *Chem. Commun.*, 2013, **49**, 8410.

5 X. Gao, J. Zhou, R. Du, Z. Xie, S. Deng, R. Liu, Z. Liu and J. Zhang, *Adv. Mater.*, 2015, DOI: 10.1002/adma.201504407.
6 X. Gui, J. Wei, K. Wang, A. Cao, H. Zhu, Y. Jia, Q. Shu and D. Wu, *Adv. Mater.*, 2010, **22**, 617.
7 L. Chen, R. Du, J. Zhang and T. Yi, *J. Mater. Chem. A*, 2015, **3**, 20547.
8 R. Du, N. Zhang, J. H. Zhu, Y. Wang, C. Y. Xu, Y. Hu, N. N. Mao, H. Xu, W. J. Duan, L. Zhuang, L. T. Qu, Y. L. Hou and J. Zhang, *Small*, 2015, **11**, 3903.
9 D. D. Nguyen, N.-H. Tai, S.-B. Lee and W.-S. Kuo, *Energy Environ. Sci.*, 2012, **5**, 7908.
10 Y. Zhao, C. Hu, Y. Hu, H. Cheng, G. Shi and L. Qu, *Angew. Chem.*, 2012, **124**, 11533.
11 R. Du, Q. Zhao, N. Zhang and J. Zhang, *Small*, 2015, **11**, 3263.
12 Y. Wu, N. Yi, L. Huang, T. Zhang, S. Fang, H. Chang, N. Li, J. Oh, J. A. Lee, M. Kozlov, A. C. Chipara, H. Terrones, P. Xiao, G. Long, Y. Huang, F. Zhang, L. Zhang, X. Lepró, C. Haines, M. D. Lima, N. P. Lopez, L. P. Rajukumar, A. L. Elias, S. Feng, S. J. Kim, N. T. Narayanan, P. M. Ajayan, M. Terrones, A. Aliev, P. Chu, Z. Zhang, R. H. Baughman and Y. Chen, *Nat. Commun.*, 2015, **6**, 6141.
13 R. Du, N. Zhang, H. Xu, N. Mao, W. Duan, J. Wang, Q. Zhao, Z. Liu and J. Zhang, *Adv. Mater.*, 2014, **26**, 8053.
14 R. Du, Z. Zheng, N. Mao, N. Zhang, W. Hu and J. Zhang, *Adv. Sci.*, 2015, **2**, 1400006.
15 S. Chen, G. He, H. Hu, S. Jin, Y. Zhou, Y. He, S. He, F. Zhao and H. Hou, *Energy Environ. Sci.*, 2013, **6**, 2435.
16 Y. Yang, Y. Deng, Z. Tong and C. Wang, *J. Mater. Chem. A*, 2014, **2**, 9994.
17 S. Qiu, B. Jiang, X. Zheng, J. Zheng, C. Zhu and M. Wu, *Carbon*, 2015, **84**, 551.
18 Y. Yang, Z. Liu, J. Huang and C. Wang, *J. Mater. Chem. A*, 2015, **3**, 5875.
19 Y. Wang, Y. Shi, L. Pan, M. Yang, L. Peng, S. Zong, Y. Shi and G. Yu, *Nano Lett.*, 2014, **14**, 4803.
20 P. Calcagnile, D. Fragouli, I. S. Bayer, G. C. Anyfantis, L. Martiradonna, P. D. Cozzoli, R. Cingolani and A. Athanassiou, *ACS Nano*, 2012, **6**, 5413.
21 N. Chen and Q. Pan, *ACS Nano*, 2013, **7**, 6875.
22 X. Gui, Z. Zeng, Z. Lin, Q. Gan, R. Xiang, Y. Zhu, A. Cao and Z. Tang, *ACS Appl. Mater. Interfaces*, 2013, **5**, 5845.
23 L. Wu, J. Zhang, B. Li and A. Wang, *Polym. Chem.*, 2014, **5**, 2382.
24 L. Wu, L. Li, B. Li, J. Zhang and A. Wang, *ACS Appl. Mater. Interfaces*, 2015, **7**, 4936.
25 S. Zhou, W. Jiang, T. Wang and Y. Lu, *Ind. Eng. Chem. Res.*, 2015, **54**, 5460.
26 A. Turco, C. Malitesta, G. Barillaro, A. Greco, A. Maffezzoli and E. Mazzotta, *J. Mater. Chem. A*, 2015, **3**, 17685.
27 B. Kong, J. Tang, Z. Wu, J. Wei, H. Wu, Y. Wang, G. Zheng and D. Zhao, *Angew. Chem., Int. Ed.*, 2014, **53**, 2888.
28 R. Du, Q. Zhao, P. Li, X. Gao and J. Zhang, 2015, under review.
29 Y. Tian, B. Su and L. Jiang, *Adv. Mater.*, 2014, **26**, 6872.
30 J. W. Long, M. S. Logan, C. P. Rhodes, E. E. Carpenter, R. M. Stroud and D. R. Rolison, *J. Am. Chem. Soc.*, 2004, **126**, 16879.
31 L. Chen, B. Wei, X. Zhang and C. Li, *Small*, 2013, **9**, 2331.
32 Y. Li, L. Li, H. Liao and H. Wang, *J. Mater. Chem.*, 1999, **9**, 2675.
33 H. Ago, Y. Ito, N. Mizuta, K. Yoshida, B. Hu, C. M. Orofeo, M. Tsuji, K.-i. Ikeda and S. Mizuno, *ACS Nano*, 2010, **4**, 7407.
34 L. Wu, Q. Li, C. H. Wu, H. Zhu, A. Mendoza-Garcia, B. Shen, J. Guo and S. Sun, *J. Am. Chem. Soc.*, 2015, **137**, 7071.
35 H. Danan, A. Herr and A. Meyer, *J. Appl. Phys.*, 1968, **39**, 669.
36 H.-P. Cong, X.-C. Ren, P. Wang and S.-H. Yu, *ACS Nano*, 2012, **6**, 2693.
37 J. Yuan, X. Liu, O. Akbulut, J. Hu, S. L. Suib, J. Kong and F. Stellacci, *Nat. Nanotechnol.*, 2008, **3**, 332.
38 H. Bi, X. Xie, K. Yin, Y. Zhou, S. Wan, L. He, F. Xu, F. Banhart, L. Sun and R. S. Ruoff, *Adv. Funct. Mater.*, 2012, **22**, 4421.
39 Y. Lu, S. Sathasivam, J. Song, W. Xu, C. J. Carmalt and I. P. Parkin, *J. Mater. Chem. A*, 2014, **2**, 12177.
40 Y. Yang, Z. Liu, J. Huang and C. Wang, *J. Mater. Chem. A*, 2015, **3**, 5875.
41 A. Lafuma and D. Quéré, *Nat. Mater.*, 2003, **2**, 457.